

ELECTRONIC SUPPORTING INFORMATION

The Formation of Cerium(III) Hydroxide Nanoparticles by a Radiation Mediated Increase in Local pH

P. Abellan^{*a,b,c} T.H. Moser,^d I.T. Lucas,^e J.W. Grate,^c J. E. Evans^f and N. D. Browning^{c,g}

^aSuperSTEM Laboratory, SciTech Daresbury Campus,
Keckwick Lane, Daresbury WA4 4AD, UK

^bInstitute for Materials Research, University of Leeds, Leeds, LS2 9JT, UK

^cPhysical and Computational Sciences Directorate, Pacific Northwest National
Laboratory, Richland, WA 99352, USA

^dDepartment of Mechanical Engineering and Engineering Mechanics, Michigan
Technological University, Houghton, MI 49931, USA

^eSorbonne Universités, UPMC University of Paris 06, CNRS, UMR 8235, LISE, Paris
75005, France

^fEnvironmental Molecular Sciences Directorate, Pacific Northwest National Laboratory,
Richland, WA 99352, USA

^gDepartment of Materials Science and Engineering, University of Washington,
Seattle, WA 98195, USA

* Author to whom all correspondence should be addressed: pabellan@superstem.org

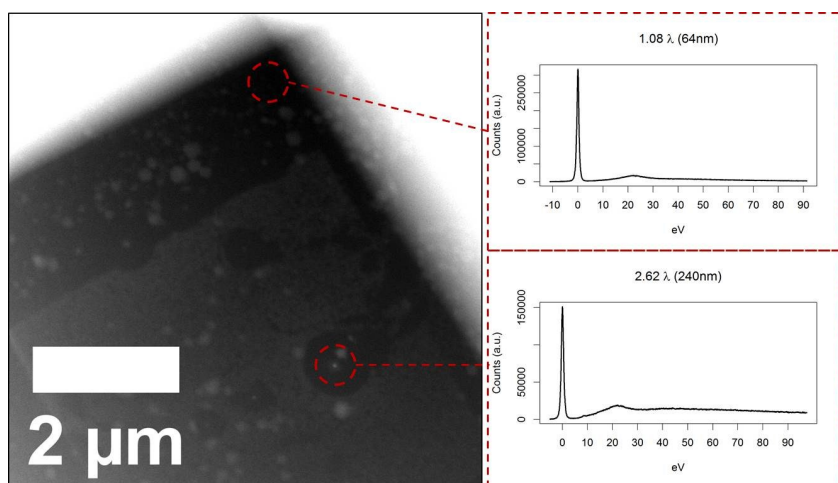
Experimental Methods

In situ HR-STEM imaging was performed with a Hummingbird Scientific fluid stage using 300 kV electrons in a FEI probe Cs-corrected Titan electron microscope equipped with an electron gun monochromator and a Gatan Quantum ERS spectrometer. HRTEM images of the deposit reaction products were acquired using an 80-300kV FEI image-corrected environmental Titan electron microscope, used in high vacuum mode. A small volume of precursor solution (0.5 μ L) was trapped within two 50nm thick silicon nitride (SiN_x) membranes supported on silicon chips (Hummingbird Scientific, Lacey, WA, USA). The presence of liquid between the membranes was confirmed by electron energy loss spectrometry (EELS) for each in situ experiment and fluid thickness was estimated, by following a procedure explained elsewhere.¹ Supporting figure S1 shows measurements taken at the cell corner and center of the irradiated area: further details are provided in the caption. The electron beam current measured in the screen dose-meter of the microscope was calibrated using an analytical holder with incorporated faraday cup (Gatan, Inc.) in order to obtain the corresponding electron current values at the

sample plane. The calibration curve measured for our microscope can be found in a previous work.² Further details on image acquisition, sample loading and on the calculation of the electron dose rates can be found in previous publications.³⁻⁸ After each in situ experiment, the chips were rinsed with DI water and let it dry on air. High-resolution images of the reaction products were then acquired in the TEM/STEM. EELS of the reaction products was also attempted in order to confirm the presence of the OH functional group in the nanoparticles, however information on the fine structure of the OK-edge was not achieved. Presumably, the relative size between the particles (2-3nm) and SN membranes (50nm), together with the beam sensitivity of the particles to the electron beam (most likely due to their small size) could be behind this limitation.

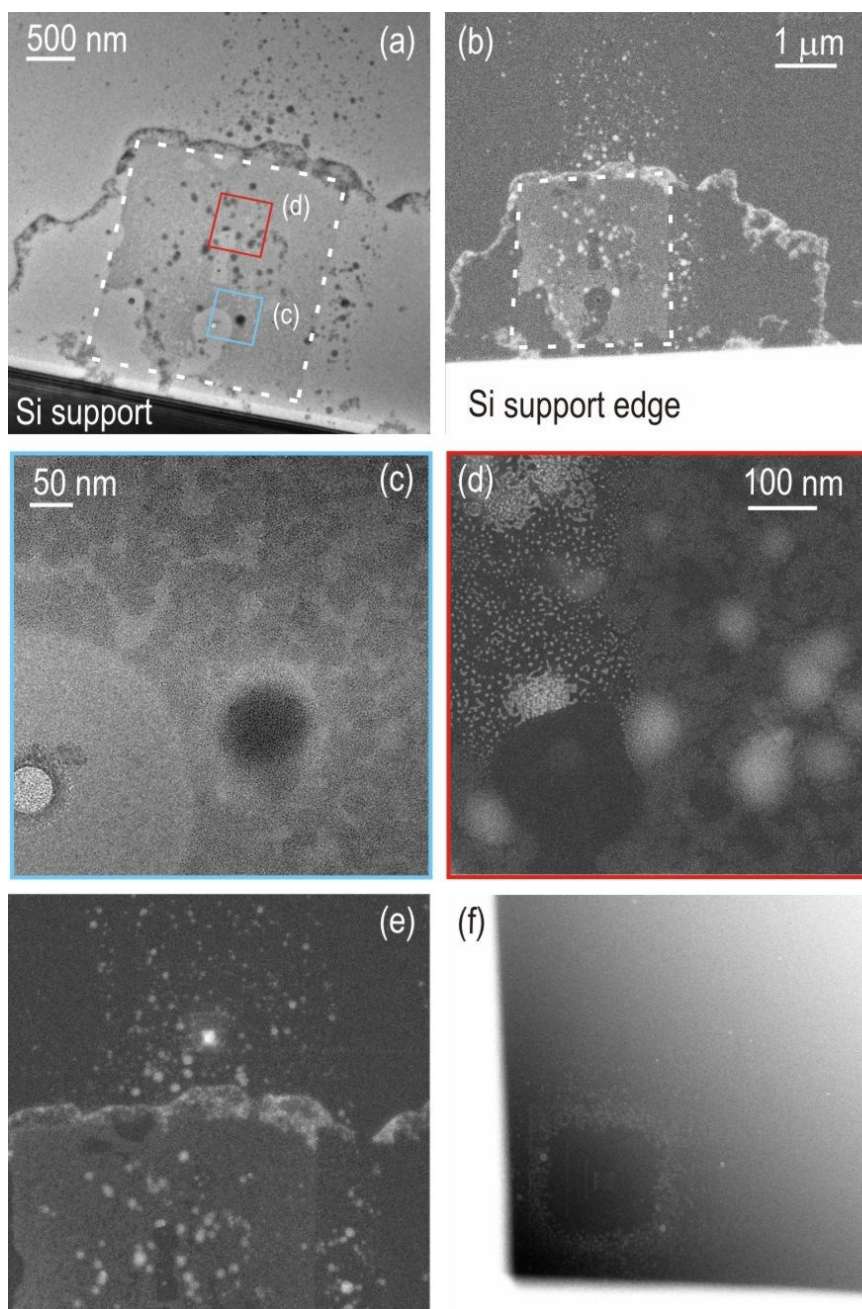
We use a precursor solution for synthesis of trivalent cerium species, following a procedure explained elsewhere.⁹ Precursor solutions were prepared by diluting cerium (III) nitrate (Sigma Aldrich), $\text{Ce}(\text{NO}_3)_3 \cdot 6\text{H}_2\text{O}$, in deionized (DI) water to a concentration of 0.1 mM. The pH of the Ce(III) precursor solution was measured to be 5.2. The pH measurement was conducted after three point calibrations (pH 4.0, 7.0 and 10.0) using a Corning pH meter 430.

Wolfram Alpha's Mathematica and code adapted from Schneider et al.¹⁰ available from Github¹¹ for TEM experiments¹⁰ was used, which we extended to include the relevant equations involving the Ce-species (see supporting table S1) and used to approximate STEM irradiation, were used to calculate the concentrations of Ce-species and the evolution of pH upon electron irradiation of the solution. Details of these calculations and all the assumptions they involve can be found in a separate section below.



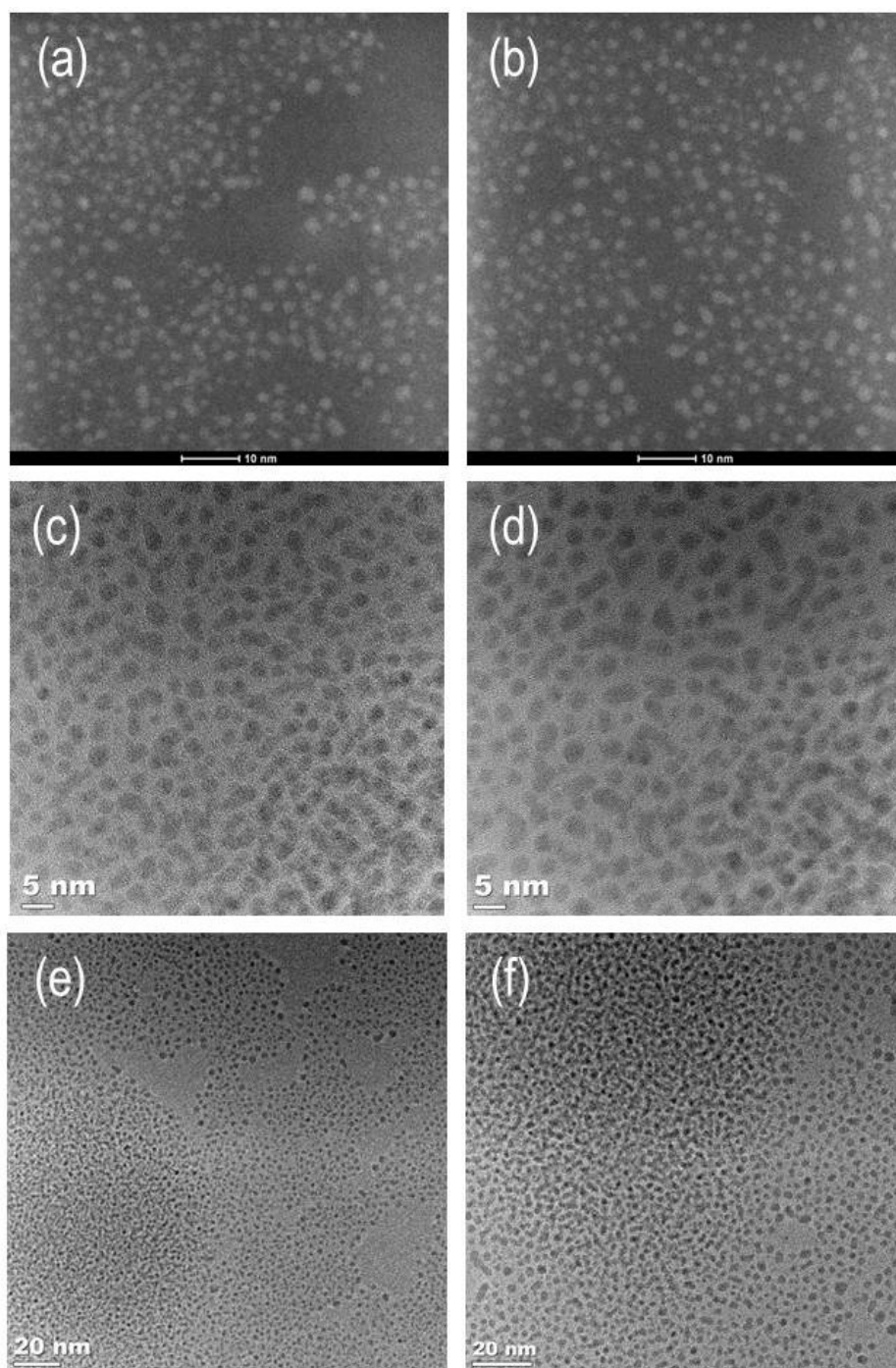
Supporting Figure S1: EEL spectra on the right were recorded directly from the liquid cell after in-situ growth. The total water thickness was estimated within 15% error approx. by following a procedure reported elsewhere.^{1, 12} The presence of two 50nm SiN_x membranes was accounted for in the calculations. The HAADF image on the left was taken after dismantling the cell and observed dry. The regions where the EEL spectra on the right hand side were recorded are indicated. Regions where particles were dissolved correspond to regions where the electron beam was left steady for a few seconds. The calculated relative thickness of $t=1.08\lambda$ (above)

and $t=2.62\lambda$ (below), where λ is the inelastic mean free path yielded total thickness values indicated. Total water thickness on the irradiated/growth area was 240 ± 40 nm.



Supporting Figure S2: (a) TEM and (b) Dark field (DF) STEM images taken after dismantling the chips and recorded dry showing low magnification views of the irradiated area (indicated with dashed lines) and the surroundings, where growth is also observed. (c) and (d) are higher magnified images of areas indicated in (a) showing the effect of parking the beam when acquiring EELS. Dissolution of particles in some areas and reorientation and agglomeration of nearby particles is observed. (e) shows the top most growth front and particles grown outside the area of in-situ observation. (f) shows a micrograph taken through the aqueous solution

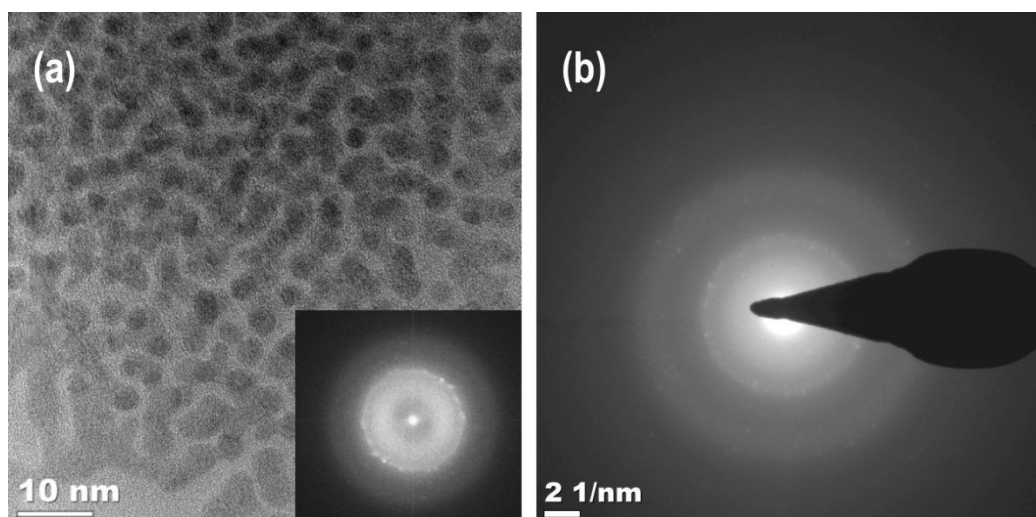
after a dissolution experiment. The empty area in the center and an agglomeration of particles formed in the surroundings can be observed.



Supporting Figure S3: (a) and (b) are DF STEM images and (c)-(f) HRTEM images of the reaction products of the particles growth experiments using the high current conditions, showing the irradiated surface of the membrane covered on nanometric particles.

Structural Characterization and Texture of Reaction Products

High resolution (HR) TEM, HR STEM images and Electron Diffraction Patterns (EDP) of the reaction products reveal that the hexagonal $\text{Ce}(\text{OH})_3$ phase was formed during the in-situ growth experiments using high beam current conditions. The EDP and FFT analysis details also revealed that the orientation of the crystals is not completely random. Figure S4 shows a HR-TEM image and its corresponding FFT, (a) and a EDP in (b) of the nanoparticles area. In both cases, the brightest diffraction ring belonged to the (-121), (2-11) and (111) reflections (with nominal inter-planar spacing of 2.47 Angstroms) as well as (2-21) and (201) and (021) reflections (nominal spacing of 2.26 Angstroms).

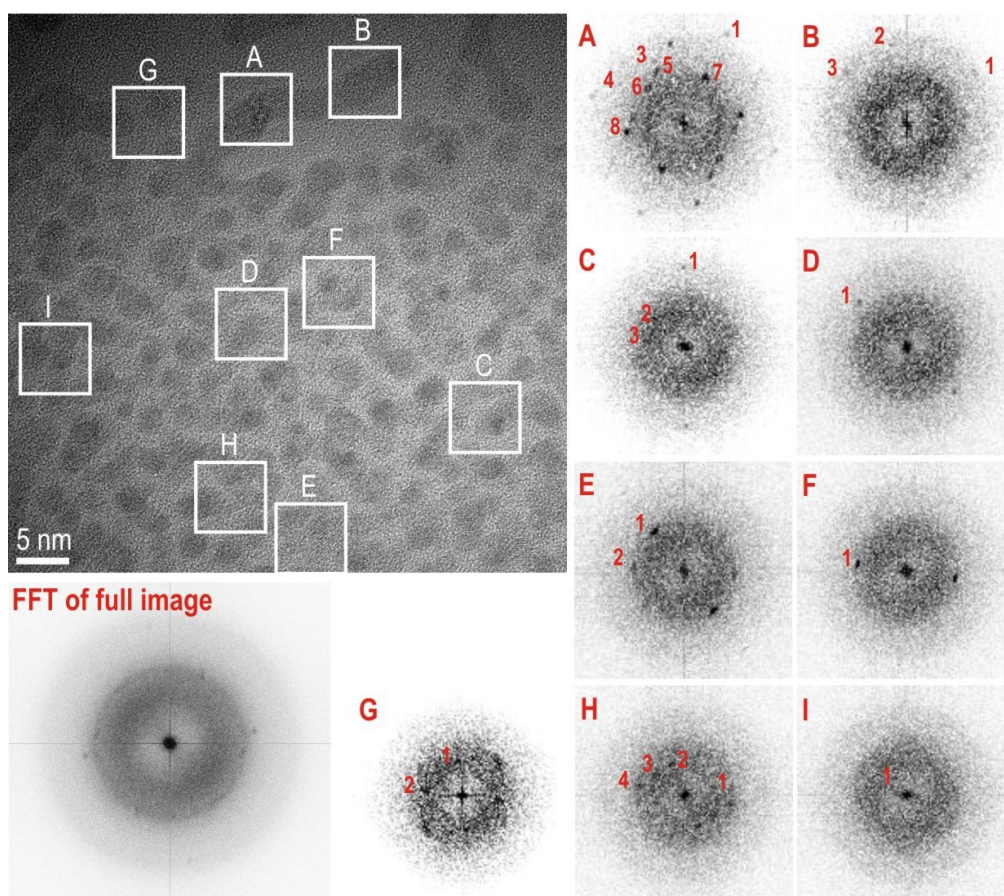


Supporting Figure S4: (a) FFT of the differently oriented $\text{Ce}(\text{OH})_3$ particles. Brightest spots are the (-121), (2-11), (111) and (2-21), (201), (021) family of planes of the hexagonal structure (with nominal spacing of 2.47 and 2.26 Angstroms respectively). Same brightest spots are observed in EDP analysis, (b).

Figure S5 shows a HR TEM image of the particles and the FFT of individual regions indicated A-I. The different reflections have measured and displayed in the following table:

Spot Index in Image	d (Experimental) [Å]	d (Nominal) [Å]	(hkl)
I1	5.45	5.620	(-110); (100); (010)
H1	3.8	3.806	(001)
H2	3.4	3.245	(-120); (2-10); (110)
G1; G2; H3	3.2; 3.1; 3.1	3.151	(-111); (1-11); (0-11); (101); (011); (-101)
C2; C3	2.79; 2.89	2.810	(200); (-220); (020)
H4	2.5	2.469	(-121); (-12-1); (11-1); (2-11); (-211); (111)
A7; A6; E1; E2 D1;	2.21; 2.27; 2.33; 2.3; 2.33	2.261	(2-21); (-221); (02-1); (20-1); (201); (021)
A8	2.00	2.124	(-130); (3-20); (210); (-230); (120); (3-10)

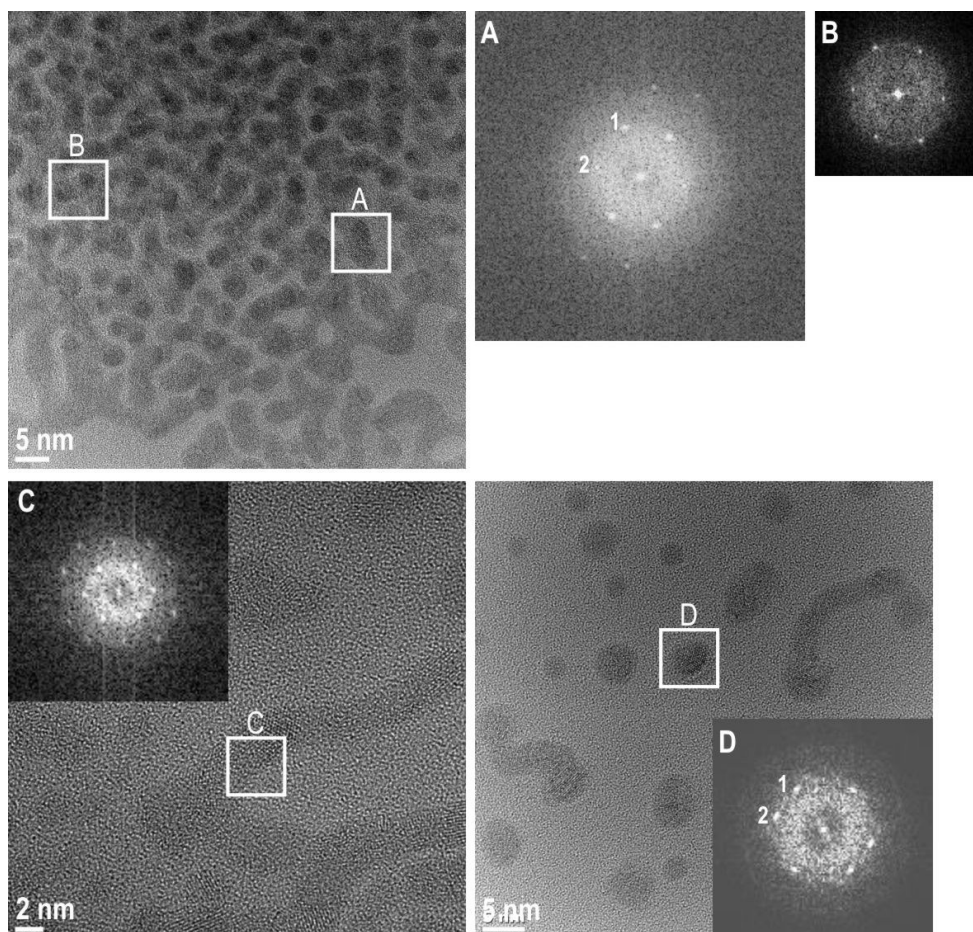
A5	1.92	1.903	(002)
A3; D1	1.67; 1.74		
A4	1.55		
B3	1.53		
C1; B2	1.43; 1.45		
A2	1.4		
B1	1.35		
A1	1.13		



Supporting Figure S5: Reaction products of the particles growth experiments using the high beam current conditions. The individual orientation in the reduced FFT of the different areas indicated as A-I in the image have been explored. The FFT of the full image shows a preferential orientation where the (-121), (2-11), (111) and (2-21), (201), (021) family of planes of the hexagonal structure appear as brightest.

As shown in Figure S5 and corresponding table, careful analysis of the HR images, where FFT analysis are performed on individual particles rather than averaging larger areas, revealed the presence of weak spots belonging to the (-110) and (100), as well as (-111) or (101) $\text{Ce}(\text{OH})_3$ reflections. In a randomly oriented distribution of particles, high intensities are expected for these families of planes. That this doesn't occur can be caused by a preferential orientation of the particles along certain zone axis. It is worth noting that also for Figure S5, when a FFT is done of the full image (also included in the figure), the brightest rings for the 2.47 and 2.26 Angstrom spacing are observed.

Figure S6 shows HR TEM images and corresponding FFT of different individual $\text{Ce}(\text{OH})_3$ crystals presenting a crystal direction almost parallel to the electron beam. The analysis of the FFTs evidence a preferential [134], [234] and [1-24] zone axis orientations, which may be caused by the effect of the electron beam. A table is provided below with an example of FFT spots measurements for crystals in the A and D regions in the HRTEM image in Figure S6.

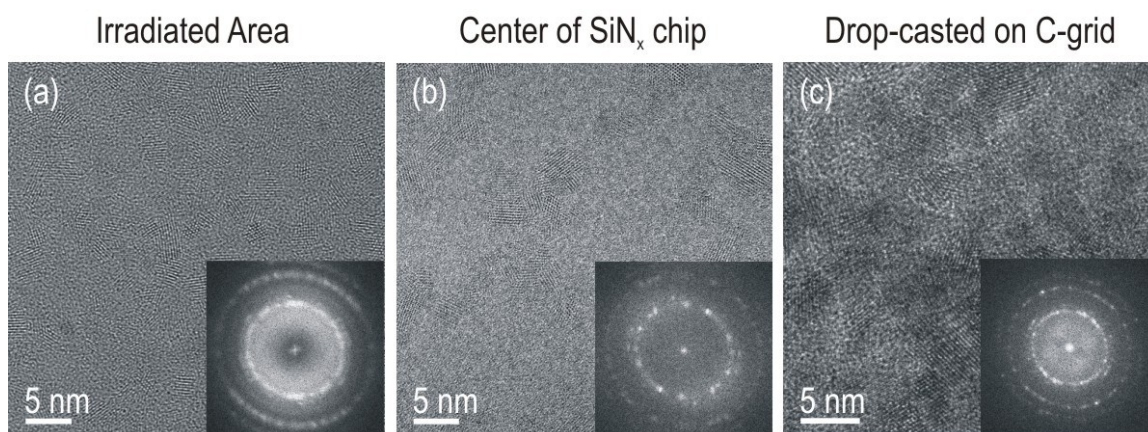


Supporting Figure S6: FFT of the differently oriented $\text{Ce}(\text{OH})_3$ particles. Brightest spots are the (102) family of planes of the hexagonal structure.

	dhkl A1 [Å]	dhkl A2 [Å]	Angle [°]	hkl #1	hkl #2	Zone Axis
Experimental	2.11	2.42	61.22			
Nominal	2.13	2.48	60.09	3-10	111	[-1-34]
	2.13	2.48	60.09	3-20	1-2-1	[23-4]
	2.13	2.48	60.09	210	2-1-1	[1-24]
	dhkl D1 [Å]	dhkl D2 [Å]	Angle [°]	hkl #1	hkl #2	Zone Axis
Experimental	2.12	2.3	55.62			
Nominal	2.13	2.27	52.5	210	021	[1-24]
	2.13	2.27	52.5	3-10	2-21	[134]
	2.13	2.27	52.5	3-20	20-1	[234]

Precipitation of cubic ($\text{CeO}_2/\text{Ce(OH)}_4$) films under low beam current conditions and when no irradiation is applied

Ex-situ high-resolution TEM (HRTEM) images were also taken after disassembly, rinsing and drying of the chips irradiated only under low beam current conditions of 6 pA, where no *in-situ* growth was observed. Images were taken for both the irradiated (Fig. S7(a)) and non-irradiated areas (Fig. S7 (b)). In both cases, nanometric crystallites of the cubic fluorite structure of ceria and most likely of its isostructural hydroxide (CeO_2 and Ce(OH)_4 , respectively) were found. In addition, similar cubic fluorite structures of ceria were found on nonirradiated surfaces of disassembled, rinsed, and dried chips from experiments at the higher beam current of 80.5 pA. As a control experiment, a solution of precursor was drop cast on a holey carbon grid. HRTEM images show that the grids were covered by similar particles (Fig. S7 (c)). These particles are in all cases precipitates that most likely form by oxidation of Ce^{3+} during the rinsing process. We note that the nanocrystalline films grown during rinsing of the chips are remarkably different from the nanoparticles resulting from the high beam current in situ experiments (Fig. 1 in main manuscript). The hexagonal Ce(OH)_3 nanoparticles formed in the beam area at 80.5 pA beam current are unambiguously distinguishable from cubic ($\text{CeO}_2/\text{Ce(OH)}_4$) films on surfaces.



Supporting Figure S7: Precipitates observed on the SiN_x membranes after rinsing the chips with DI water on both: (a) regions that had been irradiated (6 pA) and (b) regions within the same chip far from the irradiated area. (c) Pristine solution drop casted on a carbon film also showed ceria precipitates. Insets are Fast Fourier Transforms (FFT) of the images, the brightest spots corresponding to the (111) planes of the fluorite structure.

Thermodynamic Calculations

Solubility of oxygen in water:

The atmospheric pressure of O₂ has been calculated as the 20% of 10⁵ Pa, yielding 2x 10⁴ Pa. The water solubility of oxygen at 25°C and normal pressure (P= 1 bar) is 40 (mg O₂)/L water. In air, the oxygen partial pressure is 0.2 atm.

Thus, the dissolution of oxygen in water that comes in contact with air yields: 40x0.2 = **8 (mg O₂)/L**, thus 0.25 mmol L⁻¹.

Prerequisites for the construction of the Pourbaix diagram:

The Pourbaix diagram was constructed using the Nernst equation, classical approximations, and a concentration of soluble species that matches our experimental conditions C₀ = 0,1 10⁻³ mol.L⁻¹.

Note that the position of the frontiers (boundaries) between the different domains of predominance (soluble species) and existence (solids) considerably vary depending on:

- the initial concentration of cerium species C₀
- the number of species considered
- the thermodynamical equilibrium constant values used to describe the different precipitation and complexation processes.

This dependence explains the large variability between Pourbaix diagrams found in the literature for Cerium. For instance, the precipitation of Ce(OH)₃ (s) occurs at pH 10.41 for C₀ = 0,1 10⁻³ mol.L⁻¹ and for pKs_{Ce(OH)₃} = 10.76 (extracted from recent literature¹³) but drops to pH 8.3 for pKs = 21.2 extracted from the original diagram proposed by Pourbaix in 1974.¹⁴

In this section, we provide a detailed display of the equations and the thermodynamic data used for calculating the Pourbaix diagram used in this work.

The Nernst equation:

$$E = E^{\circ}_{ox/red} = \frac{RT}{nF} \cdot \log_e \left(\frac{a_{i,ox}}{a_{i,red}} \right)$$

Where: E^{°_{ox/red}}: redox potential in the standard conditions (T = 298K, p° = 1bar, a_i = 1), given vs a standard hydrogen electrode (SHE).

RT/F.log_e(X) was approximated to **0,059.log₁₀(X)**

With - R the gas constant = 8,314 J.mol⁻¹.K⁻¹

- F the Faraday constant = 96485.33 C mol⁻¹
- n the number of exchanged electrons in electrochemical half reactions
- T the temperature = 298 K

And the activities of the different species in solution including H⁺ are noted a_{i,ox} and a_{i,red}

- for solutes: a_{i(aq)} = C_i / C° = C_i with C° = 1 mol.L⁻¹ (ideal mixture of diluted salt (solute) and water solvent)
- for gas: a_{i(g)} = p_i / p° with p_i the gas partial pressure taken to 1 bar and p° the standard pressure = 1 bar)
- for solids, metals and precipitates: a_{i(s)} = 1.

The species considered to build the diagram included in the main manuscript are:

- **For Ce(IV):** precipitates like CeO₂ (s) or hydrated forms like Ce(OH)₄ (s) all solid and soluble complexes like [Ce(OH)]³⁺ (aq) and [Ce(OH)₂]²⁺ (aq). Note that Ce⁴⁺ is stable only at negative pH and therefore does not appear on the Pourbaix diagram.
- **For Ce (III):** solid Ce(OH)₃ (s) and soluble Ce³⁺ (aq)
- **For Ce(0):** cerium metal that is a solid with a_{Ce(0)} = 1.

For the calculation of the equations of the boundaries between the different domains, the concentration of the soluble specie was approximated to the initial concentration of Ce³⁺ introduced C_(aq) = C₀ = 0,1 10⁻³ mol.L⁻¹.

Pourbaix diagram boundaries between species at the same oxidation degree:

The boundaries between two species at the same oxidation degree are not potential-dependent and therefore appear as vertical lines. These lines correspond to the pH threshold for the formation of [Ce(OH)₂]²⁺ (aq), Ce(OH)₄ (s) starting from [Ce(OH)]³⁺ and Ce(OH)₃ (s) starting from Ce³⁺. These pH values have been calculated for our experimental conditions: C₀ = 0,1.10⁻³ mol.L⁻¹.

- [Ce(OH)]³⁺ / [Ce(OH)₂]²⁺ boundary:

Both species are soluble, their respective concentration are taken to C₀.

[Ce(OH)]³⁺ + OH⁻(aq) = [Ce(OH)₂]²⁺ of equilibrium constant : K⁻¹ = C₀/C₀. (Kw/[H⁺])

pH = 14 + 0.5.log (K⁻¹) = 0.72 with log k⁻¹ = log Kf_{[Ce(OH)₂]²⁺} - log Kf_{[Ce(OH)]³⁺}

- [Ce(OH)₂]²⁺ / Ce(OH)₄ boundary:

Only [Ce(OH)₂]²⁺ is soluble and its concentration taken to C₀, a_{Ce(OH)₄} = 1.

[Ce(OH)₂]²⁺ (aq) + 2OH⁻ = Ce(OH)₄ (s) of equilibrium constant : k⁻¹ = C₀ . (Kw/[H⁺])²

pH = 14 -0.5.log C₀ + 0.5.log (K⁻¹) = 4.09 with log k⁻¹ = log Kf_{[Ce(OH)₂]²⁺} + logKs_{Ce(OH)₄} = - 23.82

- Ce³⁺ / Ce(OH)₃(s) boundary:

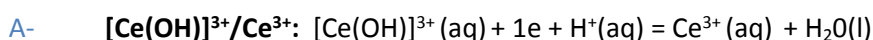
Only Ce³⁺ is soluble and its concentration taken to C₀, a_{Ce(OH)₃} = 1.

Ce(OH)₃(s) = Ce³⁺(aq) + 3.OH⁻(aq) of equilibrium constant : Ks_{Ce(OH)₃} = C₀ . (Kw/[H⁺])³

pH = 14 -1/3.log C₀ + 1/3.log Ks_{Ce(OH)₃} = 10.41 with log Ks_{Ce(OH)₃} = - 10.76

Pourbaix diagram boundaries between species at the same oxidation degree:

These boundaries are potential dependent and appear as non-vertical lines. The equation E = f(pH) of the frontiers between the different domains and the associated electrochemical half reactions are detailed in the following and compared to the one already proposed by Hayes et al.¹⁵

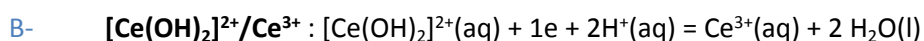


$$E = E^{\circ}_{[Ce(OH)]^{3+}/Ce^{3+}} + 0,059 \cdot \log_{10} \frac{[Ce(OH)]^{3+}}{[Ce^{3+}]} - 0,059 \cdot pH$$

$$E = E^{\circ}_{[Ce(OH)]^{3+}/Ce^{3+}} + 0,059 \cdot \log_{10} C_0/C_0 - 0,059 \cdot pH$$

$$E = 1,698 - 0,059 \cdot pH \text{ for any value of } C_0$$

$$\text{Hayes et al. (eq 14) : } E = 1,698 + 0,05916 \log_{10} \frac{[Ce(OH)]^{3+}}{[Ce^{3+}]} - 0,05916 \cdot pH$$

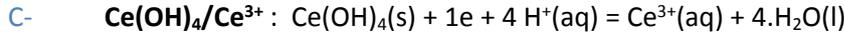


$$E = E^{\circ}_{[Ce(OH)_2]^{2+}/Ce^{3+}} + 0,059 \cdot \log_{10} \frac{[Ce(OH)_2]^{2+}}{[Ce^{3+}]} - 0,12 \cdot pH$$

$$E = E^{\circ}_{[\text{Ce}(\text{OH})_2]^{2+}/\text{Ce}^{3+}} + 0,059 \cdot \log_{10} C_0 / C_0 - 0,118 \text{ pH}$$

$$E = \mathbf{1,741 - 0,118 \text{ pH}}$$
 for any value of C_0

$$\text{Hayes et al. (eq 15)} : E = 1,741 + 0,05916 \log_{10} [\text{Ce}(\text{OH})_2]^{2+} / [\text{Ce}^{3+}] - 0,1183 \cdot \text{pH}$$

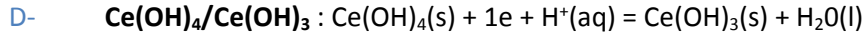


$$E = E^{\circ}_{\text{Ce}(\text{OH})_4/\text{Ce}^{3+}} - 0,059 \cdot \log_{10} [\text{Ce}^{3+}] - 0,236 \cdot \text{pH}$$

$$E = E^{\circ}_{\text{Ce}(\text{OH})_4/\text{Ce}^{3+}} - 0,059 \cdot \log_{10} C_0 - 0,236 \cdot \text{pH}$$

$$E = \mathbf{2,223 - 0,236 \cdot \text{pH}}$$
 for $C_0 = \mathbf{0,1 \cdot 10^{-3} \text{ mol} \cdot \text{L}^{-1}}$

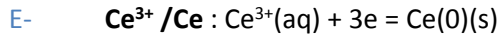
$$\text{Hayes et al. (eq 26)} : E = 1,987 + 0,05916 \log_{10} [\text{Ce}(\text{OH})_{4,\text{aq}}] / [\text{Ce}^{3+}] - 0,2366 \cdot \text{pH}$$



$$E = E^{\circ}_{\text{Ce}(\text{OH})_4/\text{Ce}(\text{OH})_3} - \mathbf{0,06 \cdot \text{pH}}$$

$$E = \mathbf{0,381 - 0,059 \cdot \text{pH}}$$
 for any value of C_0

$$\text{Hayes et al. (eq 29)} : E = 0,377 + 0,05916 \log_{10} [\text{Ce}(\text{OH})_{4,\text{aq}}] / [\text{Ce}(\text{OH})_{3,\text{aq}}] - 0,5916 \cdot \text{pH}$$

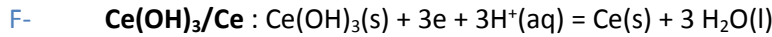


$$E = E^{\circ}_{\text{Ce}^{3+}/\text{Ce}} + \mathbf{0,02 \cdot \log_{10} [\text{Ce}^{3+}]}$$

$$E = E^{\circ}_{\text{Ce}^{3+}/\text{Ce}} + 0,02 \cdot \log_{10} C_0$$

$$E = \mathbf{-2,563}$$
 for $C_0 = \mathbf{0,1 \cdot 10^{-3} \text{ mol} \cdot \text{L}^{-1}}$

$$\text{Hayes et al. (eq 21)} : E = -2,322 + 0,01972 \log_{10} [\text{Ce}^{3+}]$$



$$E = E^{\circ}_{\text{Ce}(\text{OH})_3/\text{Ce}} - 0,059 \text{ pH}$$

$$E = \mathbf{-1,787 - 0,059 \cdot \text{pH}}$$
 for any value of C_0

$$\text{Hayes et al. (eq 24)} : E = -1,785 + 0,01972 \log_{10} [\text{Ce}(\text{OH})_{3,\text{aq}}] - 0,5916 \cdot \text{pH}$$

Equilibrium constants used for the construction of the Pourbaix diagram

Values of thermodynamic reaction constants are highly dependent on the way reactions are written and equilibrated. We therefore summarize in the following table the different equilibrium constants and associated reactions as used in this work and the source references.

Reaction	Equilibrium Constant	Ref
$\text{H}_2\text{O}(\text{l}) = \text{H}^+(\text{aq}) + \text{OH}^-(\text{aq})$	$\text{pK}_w = 14$	
$\text{Ce}(\text{OH})_3(\text{s}) = \text{Ce}^{3+}(\text{aq}) + 3 \cdot \text{OH}^-(\text{aq})$	$\text{pK}_s_{\text{Ce}(\text{OH})_3} = 14,77$	Hayes et al. ¹⁵
$\text{Ce}^{3+}(\text{aq}) + 3\text{H}_2\text{O}(\text{l}) = \text{Ce}(\text{OH})_3(\text{s}) + 3 \text{H}^+(\text{aq})$	$\log \beta_3 = -27,23$	Lee & Byrne ¹⁶
$\text{Ce}(\text{OH})_4(\text{s}) = \text{Ce}^{4+}(\text{aq}) + 4 \text{OH}^-(\text{aq})$	$\text{pK}_s_{\text{Ce}(\text{OH})_4} = 51,86$	Bilal et al. ¹³
$\text{Ce}^{4+}(\text{aq}) + 4\text{H}_2\text{O}(\text{l}) = \text{Ce}(\text{OH})_4(\text{s}) + 4 \text{H}^+(\text{aq})$	$\log k_4 = -4,124$	Hayes et al. ¹⁵
$\text{Ce}^{4+}(\text{aq}) + \text{OH}^-(\text{aq}) = [\text{CeOH}]^{3+}(\text{aq})$	$+\log K_f_{[\text{CeOH}]^{3+}} = 14,76$	Bilal et al. ¹³
$\text{Ce}^{4+}(\text{aq}) + 2 \cdot \text{OH}^-(\text{aq}) = [\text{Ce}(\text{OH})_2]^{2+}(\text{aq})$	$+\log K_f_{[\text{Ce}(\text{OH})_2]^{2+}} = 28,04$	Bilal et al. ¹³

To bridge our work to previous ones by Hayes et al., we detail here the calculation of the reactions constants starting from Gibbs free enthalpies used by Hayes et al.¹⁵

For a specific reaction, according to Hess's law, the Gibbs free energy $\Delta_r G^\circ$ can be calculated from the algebraic summation of Gibbs free energy of formation $\Delta_f G^\circ$ of the different products involved in the reactions.

Therefore for the reaction $\text{Ce(OH)}_4(\text{s}) = \text{Ce}^{4+}(\text{aq}) + 4.\text{OH}^-(\text{aq})$ (dissolution reaction)

$$\Delta_{\text{diss}} G^\circ = -\Delta_f G^\circ_{\text{Ce(OH)}_4(\text{s})} + \Delta_f G^\circ_{\text{Ce}^{4+}(\text{aq})} + 4.\Delta_f G^\circ_{\text{OH}^-} = + 1428,66 - 503,8 + 4 \times -157,2 = 296,06 \text{ KJ.mol}^{-1}$$

The Gibbs free energy $\Delta_r G^\circ$ is related to the reaction constant through the equation: $K = \exp(-\Delta_r G^\circ/RT)$, thus $K_{\text{Ce(OH)}_4} = \exp(-\Delta_{\text{diss}} G^\circ/RT) = 10^{[-\Delta_{\text{diss}} G^\circ/(2,3.RT)]} = 10^{(-51,87)}$

and $\text{p}K_{\text{Ce(OH)}_4} = 51,86$ in agreement with Bilal et al,¹³ that Hayes quotes in his work.

$K_{\text{Ce(OH)}_3}$, $K_{[\text{CeOH}]_3^+}$ and $K_{[\text{Ce(OH)}_2]_2^+}$ were calculated in a similar way:

- $K_{\text{Ce(OH)}_3}$: $\text{Ce(OH)}_3(\text{s}) = \text{Ce}^{3+}(\text{aq}) + 3.\text{OH}^-(\text{aq})$ (dissolution reaction)

$$K_{\text{Ce(OH)}_3} = \exp(-\Delta_{\text{diss}} G^\circ/RT) = 10^{[-\Delta_{\text{diss}} G^\circ/(2,3.RT)]} = 10^{(-14,77)}$$

with $\Delta_{\text{diss}} G^\circ = -\Delta_f G^\circ_{\text{Ce(OH)}_3(\text{s})} + \Delta_f G^\circ_{\text{Ce}^{3+}(\text{aq})} + 3.\Delta_f G^\circ_{\text{OH}^-} = + 1227,90 - 672,00 + 3 \times -157,2 = 84,3 \text{ KJ.mol}^{-1}$

$\text{p}K_{\text{Ce(OH)}_3} = 14,777$ consistent with the hydrolysis constant $\log \beta_3 = - 27.23$ by Lee and Byrne¹⁶ that Hayes et al. quote in his work, with $\beta_3 = (K_w)^3 / K_{\text{Ce(OH)}_3}$.

- $K_{[\text{CeOH}]_3^+}$: $\text{Ce}^{4+}(\text{aq}) + \text{OH}^-(\text{aq}) = [\text{CeOH}]^{3+}(\text{aq})$ (complex formation reaction)

$$K_{[\text{CeOH}]_3^+} = \exp(-\Delta_{\text{form}} G^\circ/RT) = 10^{[-\Delta_{\text{form}} G^\circ/(2,3.RT)]} = 10^{(-14,76)}$$

with $\Delta_{\text{form}} G^\circ = -\Delta_f G^\circ_{\text{Ce}^{4+}(\text{aq})} - \Delta_f G^\circ_{\text{OH}^-} + \Delta_f G^\circ_{[\text{CeOH}]_3^+(\text{aq})} = 503,8 + 157,2 - 745,26 = - 84,26 \text{ KJ.mol}^{-1}$

$\log_{10} K_{[\text{CeOH}]_3^+} = 14,76$ in agreement with Bilal et al,¹³ that Hayes et al. quote in his work.

- $K_{[\text{Ce(OH)}_2]_2^+}$: $\text{Ce}^{4+}(\text{aq}) + 2\text{OH}^-(\text{aq}) = [\text{Ce(OH)}_2]^{2+}(\text{aq})$ (complex formation reaction)

$$K_{[\text{Ce(OH)}_2]_2^+} = \exp(-\Delta_{\text{form}} G^\circ/RT) = 10^{[-\Delta_{\text{form}} G^\circ/(2,3.RT)]} = 10^{(-28,029)}$$

with $\Delta_{\text{form}} G^\circ = -\Delta_f G^\circ_{\text{Ce}^{4+}(\text{aq})} - 2.\Delta_f G^\circ_{\text{OH}^-} + \Delta_f G^\circ_{[\text{Ce(OH)}_2]_2^+(\text{aq})} = 503,8 + 2 \times 157,2 - 978,270 = - 160,070 \text{ KJ.mol}^{-1}$

$\log_{10} K_{[\text{Ce(OH)}_2]_2^+} = 28,059$ in agreement with 28,04 from Bilal et al,¹³ that Hayes et al quote in his work.

Standard redox potentials used for the construction of the Pourbaix diagram

We summarized here the different standard redox potential used in the calculation of Pourbaix diagram. We have also included relevant redox couples for radiation chemical synthesis in water.¹⁷

Redox couple Ox / Red	Standard potentials E°(V) vs SHE
(OH ⁻ , H ⁺) / H ₂ O	2.7
Ce(OH) ₄ / Ce ³⁺	1.987
H ₂ O ₂ / H ₂ O	1.776
Ce ⁴⁺ / Ce ³⁺	1.743
[Ce(OH) ₂] ²⁺ / Ce ³⁺	1.741
[Ce(OH)] ³⁺ / Ce ³⁺	1.698
O ₂ / H ₂ O	1.23
Ce(OH) ₄ / Ce(OH) ₃	0.381
H ⁺ /H ₂	0
Ce(OH) ₃ / Ce	-1.787
Ce ³⁺ / Ce	-2.322
Solvated e ⁻	-2.9

Standard potential value E° of the different redox-couples considered in the Pourbaix diagram are calculated from the one of Ce^{4+}/Ce^{3+} and Ce^{3+}/Ce using linear combination of chemical and half redox reactions and summation of corresponding Gibbs free enthalpies ($\Delta_{\text{electrochem}}G^\circ = -n.F. E^\circ$ for half redox reactions, $\Delta_{\text{chem}}G^\circ = -RT.\log_e K$ for chemical reactions).

The reaction $[Ce(OH)]^{3+} (aq) + 1e + H^+(aq) = Ce^{3+} (aq) + H_2O(l)$ associated to $\Delta_r G^\circ = -F. E^\circ_{[Ce(OH)]^{3+}/Ce^{3+}}$ can be decomposed in three different reactions (a)-(b)-(c):

- (a) $Ce^{4+} (aq) + OH^-(aq) = [Ce(OH)]^{3+} (aq) : \Delta_r G^\circ = -RT.\log_e Kf_{[Ce(OH)]^{3+}}$
- (b) $Ce^{4+} (aq) + 1e = Ce^{3+} (aq) : \Delta_r G^\circ = -F. E^\circ_{Ce^{4+}/Ce^{3+}}$
- (c) $H_2O(l) = H^+(aq) + OH^-(aq) : \Delta_r G^\circ = -RT.\log_e Kw$

Therefore, $-F. E^\circ_{[Ce(OH)]^{3+}/Ce^{3+}} = -F. E^\circ_{Ce^{4+}/Ce^{3+}} + RT.\log_e Kf_{[Ce(OH)]^{3+}} + RT.\log_e Kw$
and $E^\circ_{[Ce(OH)]^{3+}/Ce^{3+}} = E^\circ_{Ce^{4+}/Ce^{3+}} - 0,059.\log_{10} Kf_{[Ce(OH)]^{3+}} + 0,06.pKw = \mathbf{1,698 V}$

Similarly, $E^\circ_{[Ce(OH)2]^{2+}/Ce^{3+}}$, $E^\circ_{Ce(OH)4/Ce^{3+}}$, $E^\circ_{Ce(OH)4/Ce(OH)3}$ and $E^\circ_{Ce(OH)3/Ce}$ can be calculated :

$$E^\circ_{[Ce(OH)2]^{2+}/Ce^{3+}} = E^\circ_{Ce^{4+}/Ce^{3+}} - 0,059.\log_{10} Kf_{[Ce(OH)2]^{2+}} + 0,118.pKw = \mathbf{1,741 V}$$

$$E^\circ_{Ce(OH)4/Ce^{3+}} = E^\circ_{Ce^{4+}/Ce^{3+}} - 0,059.pKs_{Ce(OH)4} + 0,236.pKw = \mathbf{1,987 V}$$

$$E^\circ_{Ce(OH)4/Ce(OH)3} = E^\circ_{Ce^{4+}/Ce^{3+}} + 0,059.pKs_{Ce(OH)3} - 0,059.pKs_{Ce(OH)4} + 0,059.pKw \\ = 1,743 + 0,059.(14,77 - 51,86 + 14) = \mathbf{0,381 V}$$

$$E^\circ_{Ce(OH)3/Ce} = E^\circ_{Ce^{3+}/Ce} - 0,02.pKs_{Ce(OH)3} + 0,059.pKw = \mathbf{-1,787 V}$$

Reaction kinetics

Here we provide additional evidences that support the active role of redox reactions in equations (3)-(6) in the main manuscript on the increase of pH by computer modelling of the Radiation-induced changes in pH for the case of bulk solutions.

Modelling of the radiation-induced changes in the solution chemistry, with an emphasis on the evolution of Ce-species and pH has been done for STEM irradiation by adapting existing published code from Schneider et al.¹¹ originally created for TEM experiments¹⁰ to include not only the redox reactions for DI water — reactions 2 to 79 in Table S1 also used in reference ¹⁰ — but also the redox reactions involving Ce-species — reactions 80 to 87 in Table S1. Wolfram Alpha's Mathematica was used.

The effect of STEM irradiation was roughly approximated by considering an interaction volume equal to the volume comprised by a pixel size area (2.3nm x 2.3nm for the interaction volume considered to model the radiolysis for the experiment in Fig 1(a)) and thickness estimated by EELS as shown in Figure S1 (240nm in our case). For STEM, continuous irradiation of the observation area is done using a converging electron beam, with dimensions that here we approximate by the pixel size, during a time interval given by the pixel dwell time of the experiment (3μs in our case). After that, the beam moves onto a nearby area (corresponding to the next pixel location in the image) to continue the scan. We thus assume that after the initial continuous irradiation during the pixel dwell time, that same interaction volume won't be irradiated (it is "left to evolve" with no further irradiation) for a total amount of time equal to the total frame time of the STEM image. After that time, the beam will again be located on the initial position for the following exposure. We note here that modelling the radiation chemistry of the system under these assumptions implies that diffusion of species outside of the pixel volume is not accounted for and possible interactions with species generated from adjacent pixels are not taken into account neither. Besides, this is a bulk model which does not take the effect of membranes or confined volumes into account. All of these factors are expected to have an effect on the evolution of pH upon electron-beam irradiation.

Supporting Table S1: Redox reactions involving DI Water (reactions number 2 to 79 are included as in reference ¹⁰) and Cerium species considered

Reaction	Equilibria	Acidity Constant : K (25°C)
2	$H_2O \leftrightarrow H^+ + OH^-$	$K_2 = 13.999$
3	$H_2O_2 \leftrightarrow H^+ + HO_2^-$	$K_3 = 11.65$
4	$OH^- \leftrightarrow H^+ + O^{\cdot-}$	$K_4 = 11.9$
5	$HO_2^- \leftrightarrow H^+ + O_2^{\cdot-}$	$K_5 = 4.57$
6	$H^+ \leftrightarrow H^+ + e^-_{aq}$	$K_6 = 9.77$
	Chemical Reaction	Rate Constant (25°C) (M⁻¹.s⁻¹ unless specified otherwise)
7	$H^+ + OH^- \rightarrow H_2O$	$k_7 = 1.4 \times 10^{11}$
8	$H_2O \rightarrow H^+ + OH^-$	$k_8 = (k_7 \times K_2) / [H_2O] : (s^{-1})$

9	$\text{H}_2\text{O}_2 \rightarrow \text{H}^+ + \text{HO}_2^-$	$k_9 = k_{10} \times K_3 : (\text{s}^{-1})$
10	$\text{H}^+ + \text{HO}_2^- \rightarrow \text{H}_2\text{O}_2$	$k_{10} = 5.0 \times 10^{10}$
11	$\text{H}_2\text{O}_2 + \text{OH}^- \rightarrow \text{HO}_2^- + \text{H}_2\text{O}$	$k_{11} = 1.3 \times 10^{10}$
12	$\text{HO}_2^- + \text{H}_2\text{O} \rightarrow \text{H}_2\text{O}_2 + \text{OH}^-$	$k_{12} = (k_{11} \times K_2) / (K_3 \times [\text{H}_2\text{O}])$
13	$\text{e}^-_{\text{aq}} + \text{H}_2\text{O} \rightarrow \text{H}\cdot + \text{OH}^-$	$k_{13} = 1.9 \times 10^{11}$
14	$\text{H}\cdot + \text{OH}^- \rightarrow \text{e}^-_{\text{aq}} + \text{H}_2\text{O}$	$k_{14} = 2.2 \times 10^7$
15	$\text{H}\cdot \rightarrow \text{e}^-_{\text{aq}} + \text{H}^+$	$k_{15} = k_{16} \times K_6 : (\text{s}^{-1})$
16	$\text{e}^-_{\text{aq}} + \text{H}^+ \rightarrow \text{H}\cdot$	$k_{16} = 2.3 \times 10^{10}$
17	$\text{OH}\cdot + \text{OH}^- \rightarrow \text{O}\cdot^- + \text{H}_2\text{O}$	$k_{17} = 1.3 \times 10^{10}$
18	$\text{O}\cdot^- + \text{H}_2\text{O} \rightarrow \text{OH}\cdot + \text{OH}^-$	$k_{18} = (k_{17} \times K_2) / (K_4 \times [\text{H}_2\text{O}])$
19	$\text{OH}\cdot \rightarrow \text{O}\cdot^- + \text{H}^+$	$k_{19} = k_{20} \times K_4 : (\text{s}^{-1})$
20	$\text{O}\cdot^- + \text{H}^+ \rightarrow \text{OH}\cdot$	$k_{20} = 1 \times 10^{10}$
21	$\text{HO}_2\cdot \rightarrow \text{O}_2\cdot^- + \text{H}^+$	$k_{21} = k_{22} \times K_5 : (\text{s}^{-1})$
22	$\text{O}_2\cdot^- + \text{H}^+ \rightarrow \text{HO}_2\cdot$	$k_{22} = 5 \times 10^{10}$
23	$\text{HO}_2\cdot + \text{OH}^- \rightarrow \text{O}_2\cdot^- + \text{H}_2\text{O}$	$k_{23} = 5 \times 10^{10}$
24	$\text{O}_2\cdot^- + \text{H}_2\text{O} \rightarrow \text{HO}_2\cdot + \text{OH}^-$	$k_{24} = (k_{23} \times K_2) / (K_5 \times [\text{H}_2\text{O}])$
25	$\text{e}^-_{\text{aq}} + \text{OH}\cdot \rightarrow \text{OH}^-$	$k_{25} = 3 \times 10^{10}$
26	$\text{e}^-_{\text{aq}} + \text{H}_2\text{O}_2 \rightarrow \text{OH}\cdot + \text{OH}^-$	$k_{26} = 1.1 \times 10^{10}$
27	$\text{e}^-_{\text{aq}} + \text{O}_2\cdot^- + \text{H}_2\text{O} \rightarrow \text{HO}_2\cdot + \text{OH}^-$	$k_{27} = (1.3 \times 10^{10}) / [\text{H}_2\text{O}]^2 : (\text{M}^{-2} \cdot \text{s}^{-1})$
28	$\text{e}^-_{\text{aq}} + \text{HO}_2\cdot \rightarrow \text{HO}_2^-$	$k_{28} = 2.0 \times 10^{10}$
29	$\text{e}^-_{\text{aq}} + \text{O}_2 \rightarrow \text{O}_2\cdot^-$	$k_{29} = 1.9 \times 10^{10}$
30	$\text{e}^-_{\text{aq}} + \text{e}^-_{\text{aq}} + 2\text{H}_2\text{O} \rightarrow \text{H}_2 + 2\text{OH}^-$	$k_{30} = (5.5 \times 10^9) / [\text{H}_2\text{O}]^2 : (\text{M}^{-3} \cdot \text{s}^{-1})$
31	$\text{e}^-_{\text{aq}} + \text{H}\cdot + \text{H}_2\text{O} \rightarrow \text{H}_2 + \text{OH}^-$	$k_{31} = (2.5 \times 10^{10}) / [\text{H}_2\text{O}] : (\text{M}^{-2} \cdot \text{s}^{-1})$
32	$\text{e}^-_{\text{aq}} + \text{HO}_2\cdot \rightarrow \text{O}\cdot^- + \text{OH}^-$	$k_{32} = 3.5 \times 10^9$
33	$\text{e}^-_{\text{aq}} + \text{O}\cdot^- + \text{H}_2\text{O} \rightarrow \text{OH}\cdot + \text{OH}^-$	$k_{33} = (2.2 \times 10^{10}) / [\text{H}_2\text{O}] : (\text{M}^{-2} \cdot \text{s}^{-1})$
34	$\text{e}^-_{\text{aq}} + \text{O}_3\cdot^- + \text{H}_2\text{O} \rightarrow \text{O}_2 + \text{OH}^- + \text{OH}\cdot$	$k_{34} = (1.6 \times 10^{10}) / [\text{H}_2\text{O}] : (\text{M}^{-2} \cdot \text{s}^{-1})$
35	$\text{e}^-_{\text{aq}} + \text{O}_3 \rightarrow \text{O}_3\cdot^-$	$k_{35} = 3.6 \times 10^{10}$
36	$\text{H}\cdot + \text{H}_2\text{O} \rightarrow \text{H}_2 + \text{OH}\cdot$	$k_{36} = 1.1 \times 10^{11}$
37	$\text{H}\cdot + \text{O}\cdot^- \rightarrow \text{OH}^-$	$k_{37} = 1.0 \times 10^{10}$
38	$\text{H}\cdot + \text{HO}_2^- \rightarrow \text{OH}\cdot + \text{OH}^-$	$k_{38} = 9.0 \times 10^7$
39	$\text{H}\cdot + \text{O}_3\cdot^- \rightarrow \text{OH}\cdot + \text{O}_2$	$k_{39} = 1.0 \times 10^{10}$
40	$\text{H}\cdot + \text{H}\cdot \rightarrow \text{H}_2$	$k_{40} = 7.8 \times 10^9$
41	$\text{H}\cdot + \text{OH}\cdot \rightarrow \text{H}_2\text{O}$	$k_{41} = 7.0 \times 10^9$
42	$\text{H}\cdot + \text{H}_2\text{O}_2 \rightarrow \text{OH}\cdot + \text{H}_2\text{O}$	$k_{42} = 9.0 \times 10^7$
43	$\text{H}\cdot + \text{O}_2 \rightarrow \text{HO}_2\cdot$	$k_{43} = 2.1 \times 10^{10}$
44	$\text{H}\cdot + \text{HO}_2\cdot \rightarrow \text{H}_2\text{O}_2$	$k_{44} = 1.8 \times 10^{10}$
45	$\text{H}\cdot + \text{O}_2\cdot^- \rightarrow \text{HO}_2^-$	$k_{45} = 1.8 \times 10^{10}$
46	$\text{H}\cdot + \text{O}_3 \rightarrow \text{HO}_3\cdot$	$k_{46} = 3.8 \times 10^{10}$
47	$\text{OH}\cdot + \text{OH}\cdot \rightarrow \text{H}_2\text{O}_2$	$k_{47} = 3.6 \times 10^9$
48	$\text{OH}\cdot + \text{HO}_2\cdot \rightarrow \text{H}_2\text{O} + \text{O}_2$	$k_{48} = 6.0 \times 10^9$
49	$\text{OH}\cdot + \text{O}_2\cdot^- \rightarrow \text{OH}^- + \text{O}_2$	$k_{49} = 8.2 \times 10^9$
50	$\text{OH}\cdot + \text{H}_2 \rightarrow \text{H}\cdot + \text{H}_2\text{O}$	$k_{50} = 4.3 \times 10^7$
51	$\text{OH}\cdot + \text{H}_2\text{O}_2 \rightarrow \text{HO}_2\cdot + \text{H}_2\text{O}$	$k_{51} = 2.7 \times 10^7$
52	$\text{OH}\cdot + \text{O}\cdot^- \rightarrow \text{HO}_2^-$	$k_{52} = 2.5 \times 10^{10}$
53	$\text{OH}\cdot + \text{HO}_2^- \rightarrow \text{HO}_2\cdot + \text{OH}^-$	$k_{53} = 7.5 \times 10^9$
54	$\text{OH}\cdot + \text{O}_3\cdot^- \rightarrow \text{O}_3 + \text{OH}^-$	$k_{54} = 2.6 \times 10^9$

55	$\text{OH}\cdot + \text{O}_3\cdot \rightarrow \text{O}_2\cdot + \text{O}_2\cdot + \text{H}^+$	$k_{55} = 6.0 \times 10^9$
56	$\text{OH}\cdot + \text{O}_3 \rightarrow \text{HO}_2\cdot + \text{O}_2$	$k_{56} = 1.1 \times 10^8$
57	$\text{HO}_2\cdot + \text{O}_2\cdot \rightarrow \text{HO}_2^- + \text{O}_2$	$k_{57} = 8.0 \times 10^7$
58	$\text{HO}_2\cdot + \text{HO}_2\cdot \rightarrow \text{H}_2\text{O}_2 + \text{O}_2$	$k_{58} = 7.0 \times 10^5$
59	$\text{HO}_2\cdot + \text{O}\cdot \rightarrow \text{O}_2 + \text{OH}^-$	$k_{59} = 6.0 \times 10^9$
60	$\text{HO}_2\cdot + \text{H}_2\text{O}_2 \rightarrow \text{OH}\cdot + \text{O}_2 + \text{H}_2\text{O}$	$k_{60} = 5.0 \times 10^{-1}$
61	$\text{HO}_2\cdot + \text{HO}_2^- \rightarrow \text{OH}\cdot + \text{O}_2 + \text{OH}^-$	$k_{61} = 5.0 \times 10^{-1}$
62	$\text{HO}_2 + \text{O}_3^- \rightarrow \text{O}_2 + \text{O}_2 + \text{OH}^-$	$k_{62} = 6.0 \times 10^9$
63	$\text{HO}_2\cdot + \text{O}_3 \rightarrow \text{HO}_3 + \text{O}_2$	$k_{63} = 5.0 \times 10^8$
64	$\text{O}_2\cdot + \text{O}_2\cdot + 2\text{H}_2\text{O} \rightarrow \text{H}_2\text{O}_2 + \text{O}_2 + 2\text{OH}^-$	$k_{64} = (1.0 \times 10^2)/[\text{H}_2\text{O}]^2 : (\text{M}^{-3} \text{s}^{-1})$
65	$\text{O}_2\cdot + \text{O}\cdot + \text{H}_2\text{O} \rightarrow \text{O}_2 + 2\text{OH}^-$	$k_{65} = (6.0 \times 10^8)/[\text{H}_2\text{O}] : (\text{M}^{-2} \text{s}^{-1})$
66	$\text{O}_2\cdot + \text{H}_2\text{O}_2 \rightarrow \text{OH}\cdot + \text{O}_2 + \text{OH}^-$	$k_{66} = 1.3 \times 10^{-1}$
67	$\text{O}_2\cdot + \text{HO}_2^- \rightarrow \text{O}\cdot + \text{O}_2 + \text{OH}^-$	$k_{67} = 1.3 \times 10^{-1}$
68	$\text{O}_2\cdot + \text{O}_3^- + \text{H}_2\text{O} \rightarrow \text{O}_2 + \text{O}_2 + 2\text{OH}^-$	$k_{68} = (1.0 \times 10^4)/[\text{H}_2\text{O}] : (\text{M}^{-2} \text{s}^{-1})$
69	$\text{O}_2\cdot + \text{O}_3 \rightarrow \text{O}_3\cdot + \text{O}_2$	$k_{69} = 1.5 \times 10^9$
70	$\text{O}\cdot + \text{O}\cdot + \text{H}_2\text{O} \rightarrow \text{HO}_2^- + \text{OH}^-$	$k_{70} = (1.0 \times 10^9)/[\text{H}_2\text{O}] : (\text{M}^{-2} \text{s}^{-1})$
71	$\text{O}\cdot + \text{O}_2 \rightarrow \text{O}_3\cdot$	$k_{71} = 3.6 \times 10^9$
72	$\text{O}\cdot + \text{H}_2 \rightarrow \text{H}\cdot + \text{OH}^-$	$k_{72} = 8.0 \times 10^7$
73	$\text{O}\cdot + \text{H}_2\text{O}_2 \rightarrow \text{O}_2\cdot + \text{H}_2\text{O}$	$k_{73} = 5.0 \times 10^8$
74	$\text{O}\cdot + \text{HO}_2^- \rightarrow \text{O}_2\cdot + \text{OH}^-$	$k_{74} = 4.0 \times 10^8$
75	$\text{O}\cdot + \text{O}_3\cdot \rightarrow \text{O}_2\cdot + \text{O}_2\cdot$	$k_{75} = 7.0 \times 10^8$
76	$\text{O}\cdot + \text{O}_3 \rightarrow \text{O}_2\cdot + \text{O}_2$	$k_{76} = 5.0 \times 10^9$
77	$\text{O}_3\cdot \rightarrow \text{O}_2 + \text{O}\cdot$	$k_{77} = 3.3 \times 10^3 : (\text{s}^{-1})$
78	$\text{O}_3\cdot + \text{H}^+ \rightarrow \text{O}_2 + \text{OH}\cdot$	$k_{78} = 9.0 \times 10^{10}$
79	$\text{HO}_3\cdot \rightarrow \text{O}_2 + \text{OH}\cdot$	$k_{79} = 1.1 \times 10^5 : (\text{s}^{-1})$
	Cerium Reactions	
80	$(3)\text{e}^-_{\text{aq}} + \text{Ce}^{3+} \rightarrow \text{Ce}$	$k_{80} = 1.0 \times 10^9$
81	$\text{e}^-_{\text{aq}} + \text{Ce}^{4+} \rightarrow \text{Ce}^{3+}$	$k_{81} = 6.6 \times 10^{10}$
82	$\text{OH}\cdot + \text{Ce}^{3+} \rightarrow \text{Ce}^{4+} + \text{OH}^-$	$k_{82} = 3.0 \times 10^8$
83	$\text{H}\cdot + \text{Ce}^{4+} \rightarrow \text{H}^+ + \text{Ce}^{3+}$	$k_{83} = 6.5 \times 10^7$
84	$\text{O}\cdot + \text{Ce}^{3+} \rightarrow \text{Ce}^{4+} + \text{OH}^-$	$k_{84} = 7.2 \times 10^8$
85	$\text{HO}_2\cdot + \text{Ce}^{3+} + \text{H}^+ \rightarrow \text{H}_2\text{O}_2 + \text{Ce}^{4+}$	$k_{85} = 7.3 \times 10^5$
86	$\text{HO}_2\cdot + \text{Ce}^{4+} \rightarrow \text{Ce}^{3+} + \text{H}^+ + \text{O}_2$	$k_{86} = 2.7 \times 10^6$
87	$\text{Ce} + (3)\text{H}_2\text{O} \rightarrow \text{Ce}^{3+} + (3)\text{OH}^- + (3/2)\text{H}_2$	*

* Two different possibilities have been explored in order to assign a K value to reaction 87 to be incorporated in the computer simulations: **1)** Since eq. 87 is a total reaction, the products of eq. 87 were directly substituted on the right hand side of eq. 80, if we assume that the reaction is not limited by the diffusion of water. Under this approximation, the reaction: $3\text{e}^-_{\text{aq}} + \text{Ce}^{3+} \rightarrow \text{Ce}^{3+} + 3\text{OH}^- + (3/2)\text{H}_2$, with a K-value equal to that of eq. 80 in Table S1 would substitute equations 80 and 87. This option has been applied to the modelling results shown in Figure S8 and Figure 5 in the main manuscript. **2)** Alternatively, K value was arbitrarily chosen to be 'very fast' (a value of 1×10^{15} , i.e. 5 orders of magnitude larger than the fastest reaction in

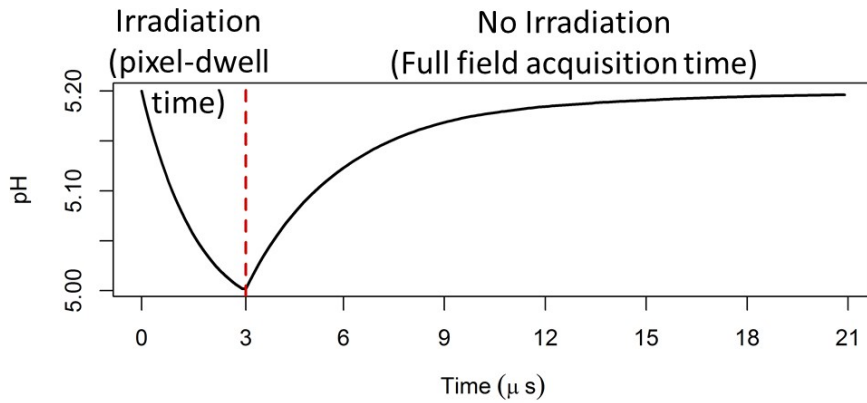
table S1). We note that a stiff system (singularity) error in Mathematica was produced if increasing the K value above 10^{25} . This option (not shown) gave similar trends to Figure S8.

STEM irradiation of pure DI water

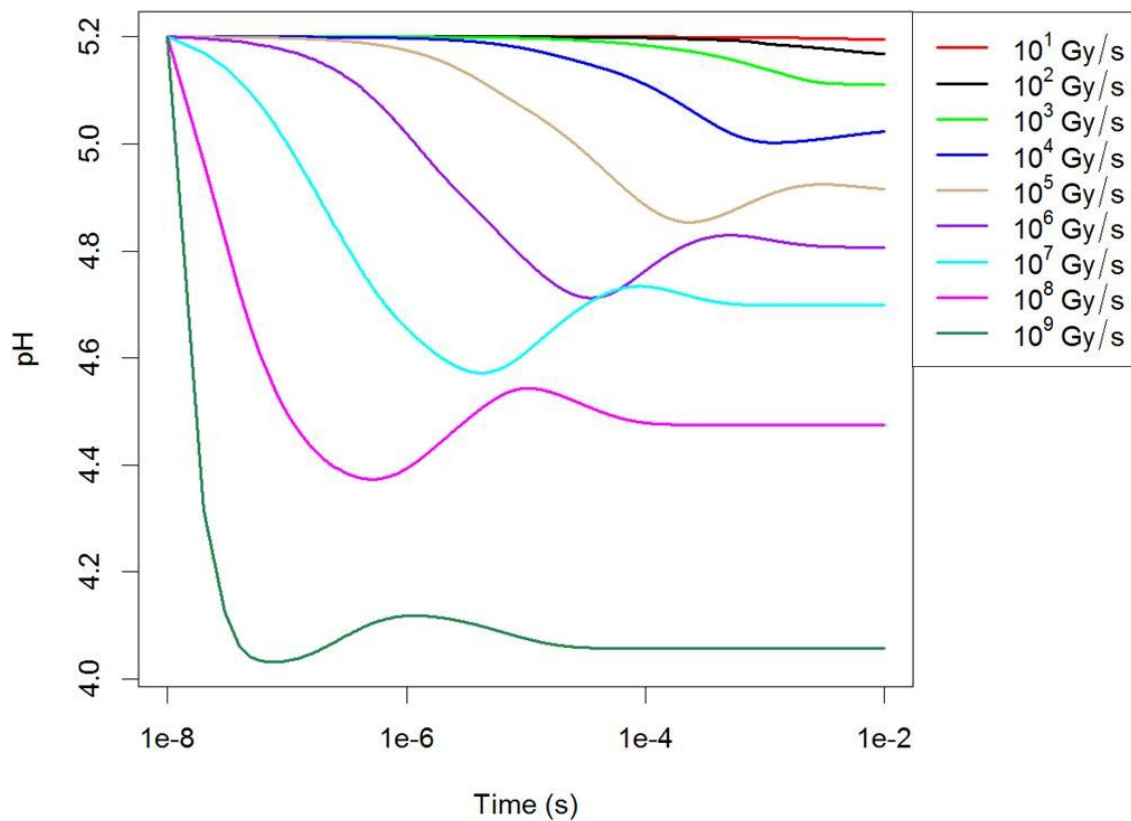
In the radiolysis of aqueous solutions by high energy electrons, radicals are generated almost entirely from the H_2O solvent molecules.^{18, 19} The primary radicals produced by the radiation of H_2O are: e^-_{aq} , H_3O^+ , $H\cdot$, $OH\cdot$, H_2 , H_2O_2 and $HO_2\cdot$.²⁰ Among these radicals, e^-_{aq} and $OH\cdot$ are the strongest reducing and oxidizing agents, where $OH\cdot$ is characterized by a large redox potential of $E^0[OH\cdot/OH^-] = 2.7$ V (in acidic solution, pH=0) and $E^0[OH\cdot/OH^-] = 1.9$ V vs SHE (in neutral solution).²¹ High energy electron irradiation of DI water typically leads to pH decrease because of the predominant formation of H_3O^+ over OH^- during water radiolysis, after the initial formation of the reductive radical $H\cdot$ and oxidizing $OH\cdot$. This trend is so for typical radiation sources and has also been confirmed for the higher doses in TEM mode¹⁰. Here, we repeat these calculations for the case of the one pixel irradiation volume for comparison with modelling when incorporating the reactions involving Ce-species (below).

Supporting Figure S8 shows the pH evolution of pure DI H_2O for a single $3\mu s$ electron beam exposure followed by 3.78s of no dose input (the time taken for the STEM probe to scan the rest of the frame). The initial values for this simulation were a pH of 5.2 and a dose within the 10^6 - 10^7 range of 4.5×10^6 Gy/s. As shown in the figure, after $3\mu s$ of irradiation, the pH decreases to a value of 5.0. It is worth noticing that the equilibrium value was at 4.99 and thus we can safely say that at $3\mu s$, equilibrium seems to have been already reached under those conditions for a pure water system. During recovery (no dose) the pH reaches a value of 5.19 by $11.5\mu s$ after irradiation and stabilizes rapidly ($t=14.6\mu s$ in the graph).

The graphs on Figure S9 show the evolution of the pH as a function of time for dose values ranging from 10^1 to 10^9 Gy/s. In this case, continuous irradiation is assumed during the entire range. Calculations are done for an initial pH of 5.2 for a time range 0-0.1s. We note that the dose we use for particle growth is about 3×10^6 Gy/s. As shown in the graphs, the pH decreases upon electron-beam irradiation and such decrease is higher for higher dosages. These results were expected and have already been shown in previous work by Schneider et al¹⁰ in a larger irradiation volume. We plot them here to make a direct comparison with the pH evolution trends we observe once the reactions accounting for the effect of Ce-species are incorporated (Figure S10).



Supporting Figure S8: pH change over time in a DI water solution including the two different irradiation regimes within a pixel size volume for an initial pH of 5.2. Time $t=0$ is the start of the pixel dwell time. Continuous irradiation of the pixel for a time lapse of $3\mu\text{s}$ is modelled followed by a second exposure regime where no dose is applied.



Supporting Figure S9: Radiolysis induced changes in pH as a function of time in DI Water for different dose values and considering a pixel area \times liquid thickness interaction volume and a starting pH of 5.2.

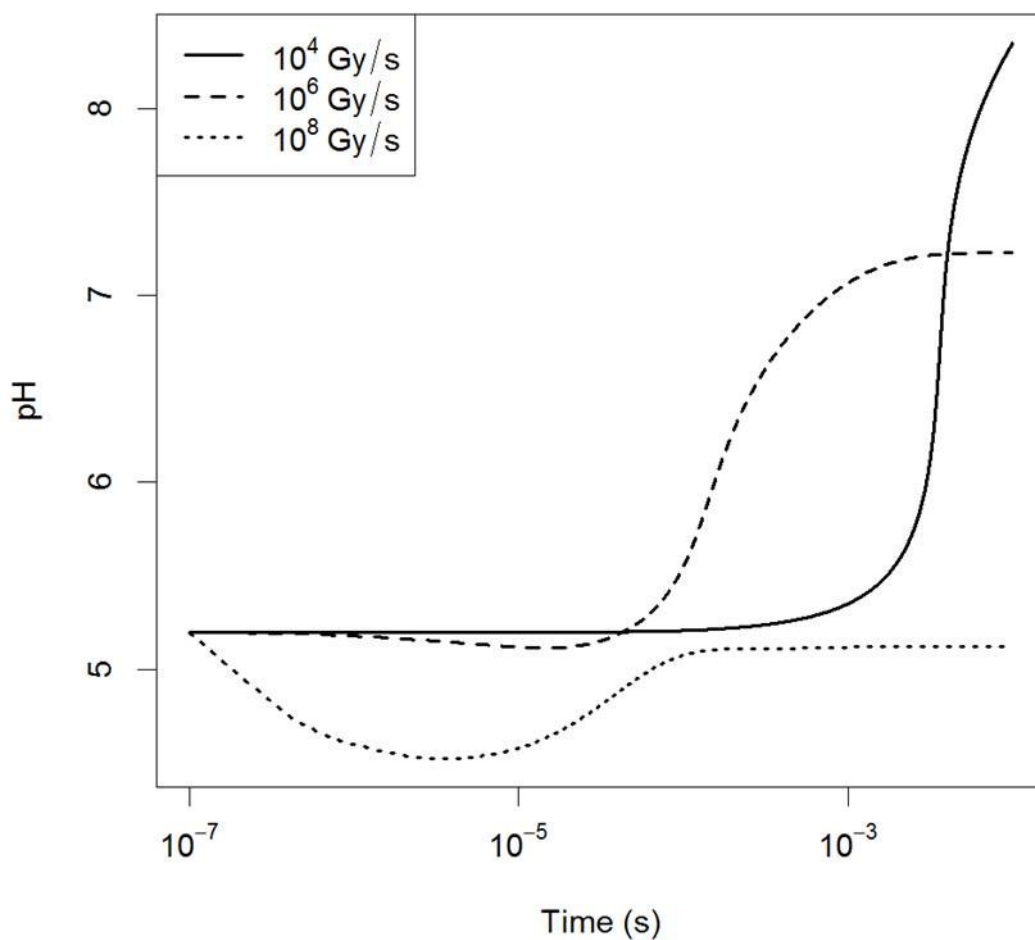
STEM irradiation incorporating the Ce-Reactions

In order to examine the proposed mechanism, involving the effect of Ce-species through equations (3)-(6) in the manuscript, computer modelling was done incorporating all equations in Table S1, including the redox reactions for Ce-species in eqs. (80)-(87).

Figure S9 shows the modelling results for the case used in the main manuscript, where the products of the total reaction 87 are directly substituted on the right hand side of eq. 80. Under this approximation, the reaction: $3e_{aq}^- + Ce^{3+} \rightarrow Ce^{3+} + 3OH^- + (3/2)H_2$, with a K-value equals to that of eq. 80 in Table S1 would substitute equations 80 and 87.

We have therefore considered in both cases that eq. (4) in the main manuscript producing Ce^0 is kinetically limiting and that as soon as Ce^0 is produced it will react with water very fast. The second case will occur immediately.

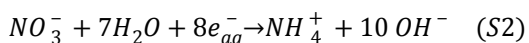
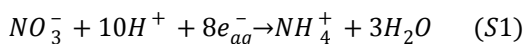
As explained in the main manuscript, in contrast to pH decreases for pure DI water, solutions containing cerium ions are observed to increase in pH, becoming alkaline within a ms of constant irradiation. It is worth noting that although the model used for the calculations qualitatively show the trends and that an increase of pH is possible by the effect of the Ce-species in the solution, a quantitative match with results was not expected due to important approximations, such as neglecting the effect of membranes and assuming a closed system with no inter-exchange of species.



Supporting Figure S10: Radiolysis induced changes in pH as a function of time in an DI water solution containing Cerium species (accounting for equations 80-87 in Table S1) for different dose values and considering a pixel area x liquid thickness interaction volume and a starting pH of 5.2.

Other Chemical Pathways that could increase the pH by the effect of Nitrate Ions and the SiN_x Membranes

Additional increase of the pH might originate from the presence of nitrate ions in the solution, following the reactions:



Previous electrochemical studies of the nitrate reduction process in aqueous media reported that for potential more negative than -1.0 V vs. SCE in 0.1M KNO₃ aqueous solution, nitrate ions would produce an increase of the interfacial pH – a pH increase from 10.5 to 12 was measured in situ.²² Similar results were found in the elaboration of ceria coatings on stainless steel by electrochemical impregnation from a cerous nitrate aqueous solution. Formation of pure CeO₂ coating at the electrode for bulk solution pH < 4 could only be explained by additional complex mechanisms such as reactions of nitrate ions at the interface.²³ A high local concentration of aqueous electrons and nitrate ions in the liquid STEM cell could explain the increase of pH^{23, 24} according to reactions (5) and (6), required for the precipitation of Ce(OH)₃ phase (note that 3 NO₃⁻ will be released for every Ce³⁺ in solution). We note that electrochemical experiments in the STEM have previously measured an in situ drop of the deposition potential upon beam exposure (down to -0.15V for 1M electrolyte solutions and 14.5pA electron beam current).²⁵

Supporting Movie 1: In-situ BF and DF STEM movie showing e-beam induced growth of Ce(OH)₃ from a 0.1mM precursor solution of Cerium (III) nitrate, Ce(NO₃)₃·6H₂O, dissolved in DI water. The movie has been speeded up to 10 x real time (Total time of 5 minutes 52 seconds). The total acquisition time per frame is 3.78 s, which also accounts for the scan flyback time occurring outside the image area. The magnification was M = 40,000 ×, the pixel-dwell time was 3μs, the calibrated beam current was 80.5 pA and the image size was 1024×1024 pixels, which corresponded to an electron dose per frame of 3 e⁻/Å².

Supporting Movie 2: In-situ BF and DF STEM movie showing e-beam induced dissolution of already formed Ce(OH)₃ (from previous growth experiments). The movie has been speeded up to 10 x real time (Total time of 1 minute 50 seconds). The total acquisition time per frame is 3.78 s, which also accounts for the scan flyback time occurring outside the image area. The magnification was M = 115,000 ×, the pixel-dwell time was 3μs, the calibrated beam current was 80.5 pA and the image size was 1024×1024 pixels, which corresponded to an electron dose per frame of 24 e⁻/Å².

References

1. K. L. Jungjohann, J. E. Evans, J. A. Aguiar, I. Arslan and N. D. Browning, *Microsc. Microanal.*, 2012, **18**, 621-627.
2. P. Abellan, L. R. Parent, N. Al Hasan, C. Park, I. Arslan, A. M. Karim, J. E. Evans and N. D. Browning, *Langmuir*, 2016, **32**, 1468-1477.
3. J. E. Evans, K. L. Jungjohann, N. D. Browning and I. Arslan, *Nano Letters*, 2011, **11**, 2809-2813.
4. T. J. Woehl, J. E. Evans, L. Arslan, W. D. Ristenpart and N. D. Browning, *Acs Nano*, 2012, **6**, 8599-8610.
5. T. J. Woehl, K. L. Jungjohann, J. E. Evans, I. Arslan, W. D. Ristenpart and N. D. Browning, *Ultramicroscopy*, 2013, **127**, 53-63.
6. L. R. Parent, D. B. Robinson, P. J. Cappillino, R. J. Hartnett, P. Abellan, J. E. Evans, N. D. Browning and I. Arslan, *Chem. Mater.*, 2014, DOI: 10.1021/cm4035209, 140127063315003.
7. P. Abellan, T. J. Woehl, L. R. Parent, N. D. Browning, J. E. Evans and I. Arslan, *Chemical Communications*, 2014, **50**, 4873-4880.
8. P. Abellan, B. L. Mehdi, L. R. Parent, M. Gu, C. Park, W. Xu, Y. Zhang, I. Arslan, J.-G. Zhang, C.-M. Wang, J. E. Evans and N. D. Browning, *Nano Letters*, 2014, **14**, 1293-1299.
9. A. S. Karakoti, P. Munusamy, K. Hostetler, V. Kodali, S. Kuchibhatla, G. Orr, J. G. Pounds, J. G. Teegarden, B. D. Thrall and D. R. Baer, *Surface and Interface Analysis*, 2012, **44**, 882-889.
10. N. M. Schneider, M. M. Norton, B. J. Mendel, J. M. Grogan, F. M. Ross and H. H. Bau, *The Journal of Physical Chemistry C*, 2014, **118**, 22373-22382.
11. NMSchneider/Radiolysis, *Journal*.
12. R. F. Egerton, *Electron Energy-Loss Spectroscopy in the Electron Microscope*, Springer, New York, 3rd edn., 2011.
13. B. Bilal and E. Müller, *Zeitschrift für Naturforschung A*, 1992, **47**, 974-984.
14. M. Pourbaix, 1974.
15. S. A. Hayes, P. Yu, T. J. O'Keefe, M. J. O'Keefe and J. O. Stoffer, *Journal of the Electrochemical Society*, 2002, **149**, C623-C630.
16. J. H. Lee and R. H. Byrne, *Geochimica et Cosmochimica Acta*, 1992, **56**, 1127-1137.
17. A. J. Bard and L. R. Faulkner, *Electrochemical Methods, 2nd ed.*; Wiley: New York, 2001.
18. J. Belloni, M. Mostafavi, H. Remita, J. L. Marignier and M. O. Delcourt, *New J. Chem.*, 1998, **22**, 1239-1255.
19. J. Belloni, *Catalysis Today*, 2006, **113**, 141-156.
20. G. V. Buxton, C. L. Greenstock, W. P. Helman and A. B. Ross, *J. Phys. Chem. Data*, 1988, **17**, 513-886.
21. D. M. Stanbury, *Advances in inorganic chemistry*, 1989, **33**, 69-138.
22. M. Nobial, O. Devos, O. R. Mattos and B. Tribollet, *Journal of Electroanalytical Chemistry*, 2007, **600**, 87-94.
23. L. Arurault, P. Monsang, J. Salley and R. Bes, *Thin Solid Films*, 2004, **466**, 75-80.
24. L. Arurault, B. Daffos and F. X. Sauvage, *Materials Research Bulletin*, 2008, **43**, 796-805.
25. A. J. Leenheer, K. L. Jungjohann, K. R. Zavadil, J. P. Sullivan and C. T. Harris, *ACS Nano*, 2015, **9**, 4379-4389.